PHYSICAL REVIEW B, VOLUME 65, 054110

Hysteresis in YH_x films observed with *in situ* measurements

A. Remhof, J. W. J. Kerssemakers, S. J. van der Molen, and R. Griessen
Faculty of Sciences, Division of Physics and Astronomy, Vrije Universiteit, De Boelelaan 1081, 1081 HV Amsterdam, The Netherlands

E. S. Kooij
Faculty of Applied Physics, MESA+ Research Institute, University of Twente, P.O. Box 217, 7500 AE Enschede, The Netherlands

(Received 11 June 2001; revised manuscript received 21 August 2001; published 14 January 2002)

Giant hysteretic effects in the YH_x hydrogen switchable mirror system are observed between $x=1.9$ and $x=3$ in pressure composition isotherms, optical and electrical properties, and mechanical stress. Polycrystalline Y films are studied by simultaneous *in situ* measurements of electrical resistivity, optical transmittance and x-ray diffractometry. These experiments are linked to optical microscopy of the samples. During hydrogen loading above $x=1.9$ the films stay in the metallic fcc phase until the optical transmittance reaches its minimum and the electrical resistance curve exhibits a characteristic feature at $x=2.1$. Upon further loading the system crosses the miscibility gap in which the fcc phase coexists with the hcp phase before hydrogen saturation is reached in the pure hcp phase. While the fcc phase stays at a concentration of $x=2.1$ in the coexistence region during *loading*, it remains at a concentration of $x=1.9$ during *unloading*. The hysteretic effects observed in optical transmission and electrical resistivity result from the different properties of the *low concentration* fcc phase $YH_{1.9}$ and the high concentration fcc phase $YH_{2.1}$. They can be explained on the basis of the bulk phase diagram if the different stress states during loading and unloading are taken into account. These results contradict earlier interpretations of the hysteresis in thin film YH_x, based on nonsimultaneous measurements of the optical and structural properties on different films.

DOI: 10.1103/PhysRevB.65.054110 PACS number(s): 64.70.Kb, 68.55.−a, 61.10.−i, 78.66.Bz

I. INTRODUCTION

As a result of its large mobility and solubility hydrogen in metals can be used as a probe and/or as a functional agent in high technology materials. Prominent examples include the hydrogen-induced tuning of the magnetic exchange coupling in Fe/Nb (Ref. 1) and Fe/V (Ref. 2) super-lattices, the nondestructive measurement of the thin film-substrate interaction[3] as well as hydrogen switchable mirrors.[4] The optical properties of these switchable mirror materials as well as their electrical properties can be continuously controlled by the concentration of incorporated hydrogen. While they are shiny metallic at low hydrogen concentrations, they are transparent insulators at high hydrogen concentrations. The rapidity of this optical transition and its reversibility fueled the hope for industrial applications.[5] The yttrium-hydrogen system is the prototype for these materials. As hysteretic behavior always degrades the functioning of a technological material, its origin has to be understood in order to improve the performance of the system. The understanding of hysteresis is also a key ingredient in the study of the metal-insulator transitions in these systems.

Depending on hydrogen concentration, the yttrium-hydrogen system exhibits three structural phases.[6] The structural phase transitions are accompanied by changes in the electronic configuration, affecting the optical properties of the material.[7] Here we focus on the transition between the cubic dihydride (β) and the hexagonal trihydride (γ) phase

YH_2 crystallizes in the CaF_2 structure in which, in the ideal case, all interstitial sites with tetrahedral symmetry of the fcc metal lattice are filled with hydrogen.[8] However, impurities and structural defects as grain boundaries cause a stoichiometric deficiency $YH_{2-\delta}$ of up to $\delta=0.2$ for the stable dihydride. By occupying interstitial sites with octahedral symmetry (O sites) additional hydrogen can be accommodated within this structure until the solubility limit is reached. The stoichiometric deficiency as well as the solubility limit depend on the sample quality. From electrochemical experiments we know that the stoichiometric deficiency of our films in the β phase is $\delta=0.1$.[9] At room temperature YH_2 is metallic with a 5 times higher conductivity than that of pure yttrium metal.[6,4] Within the red part of the visible spectrum YH_2 is weakly transparent. Detailed studies of the optical properties have been carried out in the past.[10] They could be interpreted by conventional, self-consistent one-electron band structure calculations.[11]

At higher H concentration the Y-H system undergoes a structural phase transition to the hexagonal γ phase. The details of this structure are still subject of discussion.[12] As for other substoiciometric RE trihydrides,[6,13] the electronic properties of $YH_{3-\delta}$ are highly sensitive to the actual hydrogen concentration. This is nicely illustrated by the results of Hoekstra *et al.*[14] who focussed on the continuous metal-insulator transition near $x=2.86$ in thin YH_x films.

Bulk samples suffer from the aforementioned phase transitions. The specimens embrittle and are chemically unstable. In ambient air they decompose by forming hydroxides. However, these problems can be overcome in *c*-axis textured thin films, protected by a suitable cap layer. As the lattice parameter changes during the phase transitions are highly anisotropic, affecting mainly the *c* axis, a film can freely expand and contract. As a result the β-γ transition is reversible in thin films.[4,15,16]

A recent study by Kooij *et al.*[9] led to the following remarkable results. The pressure-composition isotherms be-

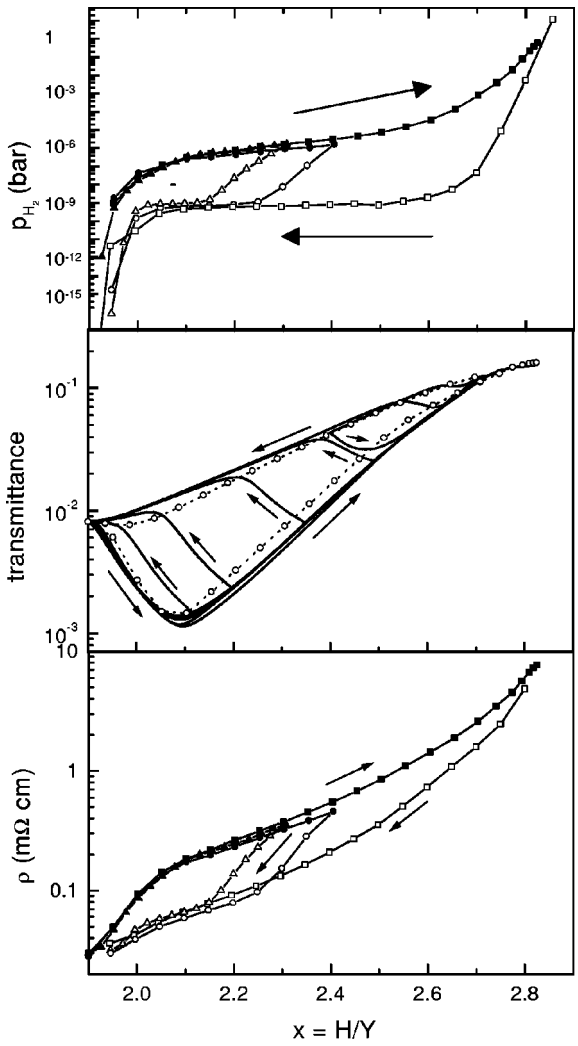

FIG. 1. The hysteresis in the Y-H_x system between $x=1.9$ and $x=2.9$ as observed in a 300 nm thick polycrystalline Y film evaporated on SiO_2 at room temperature. The H concentration is varied electrochemically. The top panel displays the pressure-composition isotherm, the one in the middle the optical transmission of the red light of a diode ($h\nu=1.96$ eV), and the one on the bottom of the electrical resistivity. All measurements are carried out at room temperature. The data in this figure are taken from Ref. 9.

tween $x=2$ and $x=3$ for absorption and desorption differ by about three orders of magnitude in pressure. Also other properties such as the optical transmittance and electrical resistivity as well as the stress state[17] depend on the history of the sample (see Fig. 1). On the basis of (i) electrochemical loading experiments, where the optical transmittance and the electrical resistivity were measured as a function of hydrogen concentration and (ii) separate gas loading experiments in which x-ray diffraction experiments were carried out together with measurements of the electrical resistivity, Kooij *et al.*[9] proposed a phase diagram for the loading branch of the solubility isotherms that differed markedly from that of bulk[6] YH_x. There is only a narrow coexistence region of the cubic and the hexagonal phase, i.e., for $1.9 \leqslant x \leqslant 2.1$. Above $x=2.1$ the YH_x film is in the pure hexagonal phase. For the unloading leg of the hysteresis loop the system is in a two phase region for $2.7 \geqslant x \geqslant 1.9$ as described in the literature.[6] The disturbingly large difference in phase coexistence in films and in bulk claimed by Kooij *et al.* provided the motivation to perform a series of new experiments in which transmittance, resistivity and crystal structure are all measured *simultaneously on one and the same sample* during loading in a hydrogen atmosphere.

In addition, these measurements are related to microscopic images of the sample recorded *in situ* in order to spatially resolve various optical phases and to monitor their behavior upon hydrogen loading and unloading. The optical images are cross-linked to the x-ray data via the electrical resistivity and the averaged optical transmission. Our results, which have the advantage to have been derived from simultaneous measurements of optical, electronic and structural properties do not confirm the existence of the small β-γ coexistence region proposed by Kooij *et al.*[9] Our results can be understood on the basis of the bulk phase diagram if the different stress states during loading and unloading are taken into account.

II. SAMPLE PREPARATION AND EXPERIMENTAL METHODS

The samples are prepared via *e*-gun evaporation in an ultra high vacuum system (background pressure below 10^{-9} mbar). We deposit Y films with a typical thickness of about 300 nm at a rate of 0.05 nm/s on polished amorphous SiO_2 (Suprasil 1, Heraeus) substrates, kept at room temperature. The resulting films are polycrystalline, *c* axis textured and posses a typical roughness of about 8 nm.[18] To protect the films from corrosion and to facilitate hydrogen uptake they are covered with a 10 to 15 nm thick Pd layer, deposited under the same conditions.

Structural characterization is performed via high angle x-ray scattering using the radiation of a rotating Cu target of a 12 kW Rigaku x-ray generator. For *in situ* studies of the structural changes upon hydrogenation a high vacuum vessel, equipped with a gas handling system, beryllium windows, electrical feedthroughs, a standard red diode, and a light detector and temperature control was used. Within that vessel the sample is mounted with its surface perpendicular to the scattering plane to measure the *c*-axis lattice parameter during hydrogenation. The vacuum chamber itself is mounted on the sample axis of a standard two-axes spectrometer. The second axis carries a highly oriented pyrolytic graphite monochromator whose (002) reflection is used to select the $K\alpha$ wavelength ($\lambda=1.542$ Å) from the diffracted beam. Within the angular range of the measurements a resolution of 0.004° is reached. The light transmitted through the sample is measured with a conventional photodiode in conjunction with a linear current to voltage amplifier. In addition, a four point van der Pauw[19] setup allows recording of the electrical resistivity. A schematical drawing of the experimental arrangement is given in Fig. 2.

Macroscopically, the optical appearance of the sample is examined with an optical microscope (Olympus BX60F5). The sample is mounted in a hydrogen loading cell with optical windows, a temperature control system and electrical

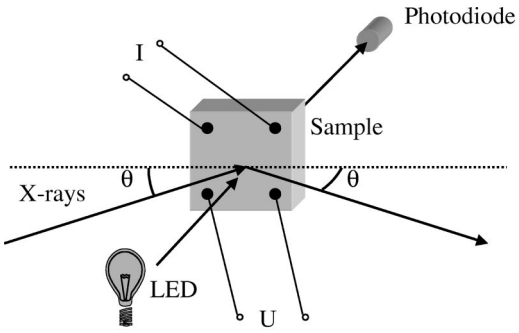

FIG. 2. Schematic representation of the experimental setup used for the simultaneous x-ray diffraction, electrical resistivity and optical transmittance measurements.

feedthroughs can be mounted onto the positioning table of the optical microscope. Using a white lamp behind the cell, optical transmission changes are monitored by means of a three-CCD red-green-blue (RGB) color camera (Sony DXC-g50P). This camera possesses a CCD chip with an array of 582 by 782 pixels. At the chosen magnification each image depicts a $1.6\times1.2\,\mathrm{mm}^2$ area of the sample. For small magnifications the spatial resolution of $2\times2\ \mu\mathrm{m}^2$ is determined by the pixel size of the camera. The camera records 25 pictures per second, guaranteeing a high temporal resolution.

III. EXPERIMENTAL RESULTS

Exposing an as-prepared Pd capped Y film to a hydrogen pressure of 1 bar results in rapid hydrogen loading up to the hexagonal γ phase.[4] Subsequent heating to 120 °C in ambient air partially desorbs the hydrogen from the sample, leaving it in the cubic β phase. This standard way of preparing dihydride samples is for example described in Ref. 6. It reflects the fact that the dihydride is thermodynamically very stable. As shown by Hayoz *et al.* much higher temperatures have to be used to desorb all the hydrogen, and regain the pure metal.[16]

Starting with a dihydride sample prepared in such a way, the temporal evolution of its radial x-ray diffraction curves, optical transmittance and electrical resistivity upon hydrogenation is depicted in Fig. 3 (from bottom to top). At $t=0$ only the (111) reflection of the dihydride phase at $2\theta=29.6°$ appears above the background. The corresponding lattice constant of 5.21Å coincides with the literature value.[6] As in the results of Kooij *et al.*,[9] the film is partially transparent for the red light of the diode ($\lambda=640\,\mathrm{nm}$). The transmittance of 1.7% as well as the initial resistivity of 31 $\mu\Omega\,\mathrm{cm}$ agree with published data on similar samples. Compared to bulk samples however the resistivity is quite high. We attribute this to electron scattering from structural defects such as grain boundaries, stacking faults and dislocations. This is confirmed by recent measurements by Enache[20] on epitaxial YH_2 films for which $\rho=18\,\mu\Omega\,\mathrm{cm}$ at room temperature. In order to follow the hydrogenation process from the cubic phase to the hexagonal phase in detail, a hydrogen pressure of 30 mbar is applied at $t=0.65\,\mathrm{h}$. Immediately the transmission starts to drop, the resistivity begins to increase and the out-of-plane lattice parameter of the β phase shrinks.

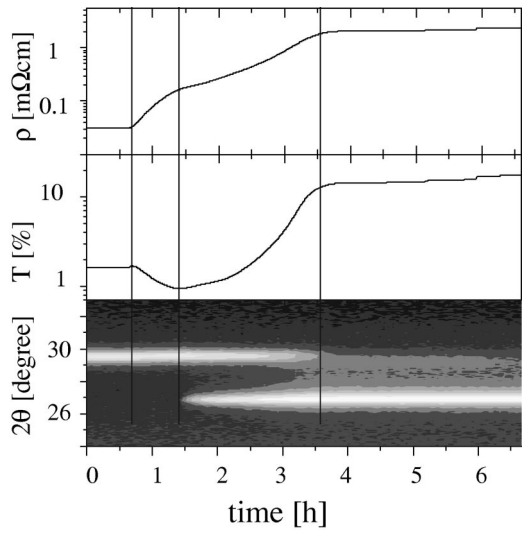

FIG. 3. Sequence of longitudinal x-ray scans (Cu K_α radiation) during the gas phase hydrogen loading of a Pd (10 nm) capped Y (300 nm) layer grown on amorphous quartz (lower panel). The reflection at 27° originates from the γ-YH_3 (0002) planes, the one at 29.6° from the β-YH_2 (111) planes. The upper and lower panel display the concurrently measured electrical resistivity and transmission for red light, respectively.

Until the first precipitations of the γ phase occur in the x-ray spectra, the lattice parameter of the cubic β phase contracts by 0.008 ± 0.004 Å or by 0.15 ± 0.075 %, the resistivity increases to about 0.2 $\mathrm{m}\Omega\,\mathrm{cm}$ and the transmission drops to 0.9%. The nucleation of the structural γ phase can be identified in the x-ray spectra by its (002) reflection at 27°. In the temporal evolution of the system the first occurrence of the γ phase, in other words the beginning of the two phase coexistence region, matches the minimum of the transmittance and the inflexion of the resistivity curve. As the hydrogenation continues, the intensity of this reflection rises monotonously and the transmittance and the resistivity increase until at $t=3.5\,\mathrm{h}$ the resistivity saturates at 2.05 $\mathrm{m}\Omega\,\mathrm{cm}$ and the transmission at 14%. At that time the intensity of the Bragg reflection of the β phase lies below the background. Increasing the hydrogen pressure in the cell to 60 mbar (at $t=5.1\,\mathrm{h}$) and later to 900 mbar (at $t=5.9\,\mathrm{h}$) causes further increase of the transmission to 15.5 and 17.3 % and of the resistivity (to 2.15 and 2.35 $\mathrm{m}\Omega\,\mathrm{cm}$, respectively), leaving the x-ray spectra unaffected. According to the pressure composition isotherm in Fig. 1, the respective equilibrium concentrations are $x=2.80$ at a pressure of 60 mbar and $x=2.84$ at 900 mbar. An influence of the hydrogen concentration on the *c*-axis lattice parameter within the hexagonal γ phase could not be detected.

The absolute transmittance values for the $YH_{1.9}$ and the $YH_{3-\delta}$ sample agree with the values measured earlier, however, our minimum is not as pronounced as observed by Kooij *et al.*[9] We attribute this to unhomogeneous loading. While some domains still get darker within the β phase, others already switched to the γ phase. Inhomogeneous loading is a general disadvantage of gas phase loading, as the applied pressure lies above the plateau pressure in the pres-

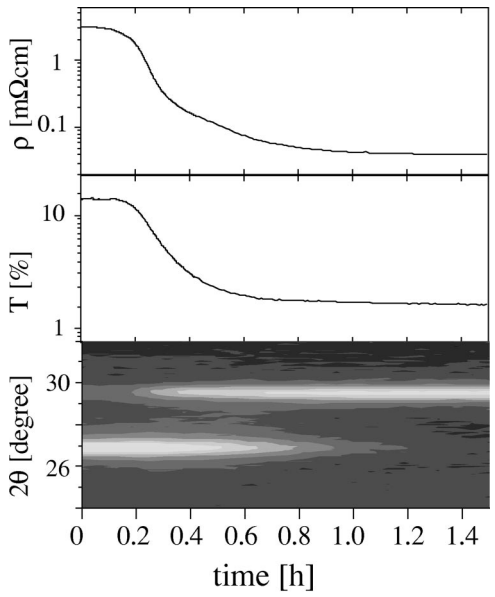

FIG. 4. Sequence of longitudinal x-ray scans (Cu K_α radiation) during hydrogen unloading of the same sample as in Fig. 3.

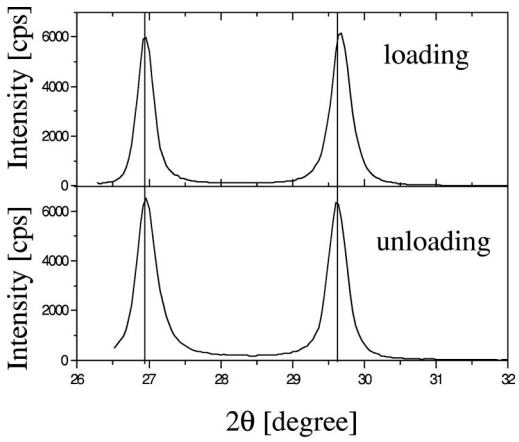

FIG. 5. Comparison of x-ray spectra in the phase coexistence region during loading (upper panel) and unloading (lower panel). Note that in both cases the γ-YH_3 (0002) reflection peaks at the same value of 27°, while the exact position of the β-YH_2 (111) reflection at about 29.6° depends on the history of the sample.

sure composition isotherm. Therefore the gas phase loading is a dynamic process in which the system relaxes to its equilibrium subsequent to hydrogen exposition. Electrochemical loading is different in this respect. During electrochemical loading the hydrogen concentration is increased stepwise, in a controlled manner, resulting in a more homogeneous loading.

Annealing the sample in ambient air at 120 °C partially drives out the hydrogen, reestablishing the β phase. As soon as the sample enters the coexistence region the transmittance as well as the resistivity fall monotonically until they reach their initial values. Figure 4 displays the x-ray diffraction curves, the transmittance and the electrical resistivity (from bottom to top) during hydrogen unloading. Unlike the loading process there are no pronounced changes within the structural β phase. Both the electrical resistivity and the transmittance are close to their equilibrium values as the intensity of the $YH_{3-\delta}$ (0002) peak drops below the background level. In particular there is no minimum within the transmittance curve. There is also another difference between loading and unloading. As displayed in Fig. 5 the lattice constant of the β phase within the two phase coexistence region depends on whether a measurement is carried out during loading or unloading. During hydrogenation the β phase first shrinks slightly until the γ phase starts to form. When both phases coexist the β phase stays with a compressed lattice. During the whole unloading process on the other hand, the β phase always exhibits its uncompressed lattice constant. In other words during loading we observe the coexistence of $YH_{3-\delta}$ with $YH_{2.1}$ and during unloading the coexistence of $YH_{3-\delta}$ with $YH_{1.9}$. We assume here that $x=1.9$ and $x=2.1$ correspond to the low and upper concentration limits for the β phase, respectively. In the next section this assumption will be justified. The same conclusion was drawn by Dornheim *et al.* from *in situ* synchrotron x-ray diffraction during electrochemical loading.[21]

As the optical properties within the β phase depend on the hydrogen concentration, the optical appearance of a similar sample is also investigated during hydrogen loading and unloading. Figure 6 shows a loading/unloading sequence performed at a temperature of 70 °C and a hydrogen pressure of 50 mbar (loading). This temperature is chosen to speed up hydrogen unloading which is very slow at room temperature. Each picture shows a $1.6\times1.2\,mm^2$ area of the film. Due to the enhanced temperature and the higher hydrogen pressure, the hydrogenation process is faster than in the previous investigation. However, the temporal resolution of the camera still allows a detailed study of the transformations within the optical appearance of the sample. At $t=0$ the film is optically homogeneous and reddish transparent. The addition of hydrogen first reduces the transmittance of the film before a more transparent phase starts to precipitate at $t=8$ min, causing the average transmittance to rise again. At that moment the simultaneously recorded resistivity, which has risen by about one order of magnitude as compared to its initial value, also changes its slope. In the previous measurement this marks the beginning of the two phase region. Thus the new phase can be identified as the hexagonal γ phase. With increasing time more and more γ phase domains nucleate, while at the same time the optical transmittance of the already nucleated γ phase domains gradually increases. Note that during hydrogen loading the γ phase coexists with a black, low transparency β phase. Later in the discussion this will be identified as $YH_{2.1}$.

Expelling the hydrogen from the sample at an intermediate state ($t=9$ min), thus going from the loading leg to the unloading leg by replacing the hydrogen atmosphere with ambient air first influences only the β phase. Its transparency increases back towards its initial value, leaving the γ phase unaffected. As a result the overall transparency increases. As soon as the β phase reaches its equilibrium, the γ phase transforms back to the β phase. Therefore, during unloading, the γ phase coexists with a reddish, relatively transparent β phase. Reloading the film with hydrogen at $t=39$ min again

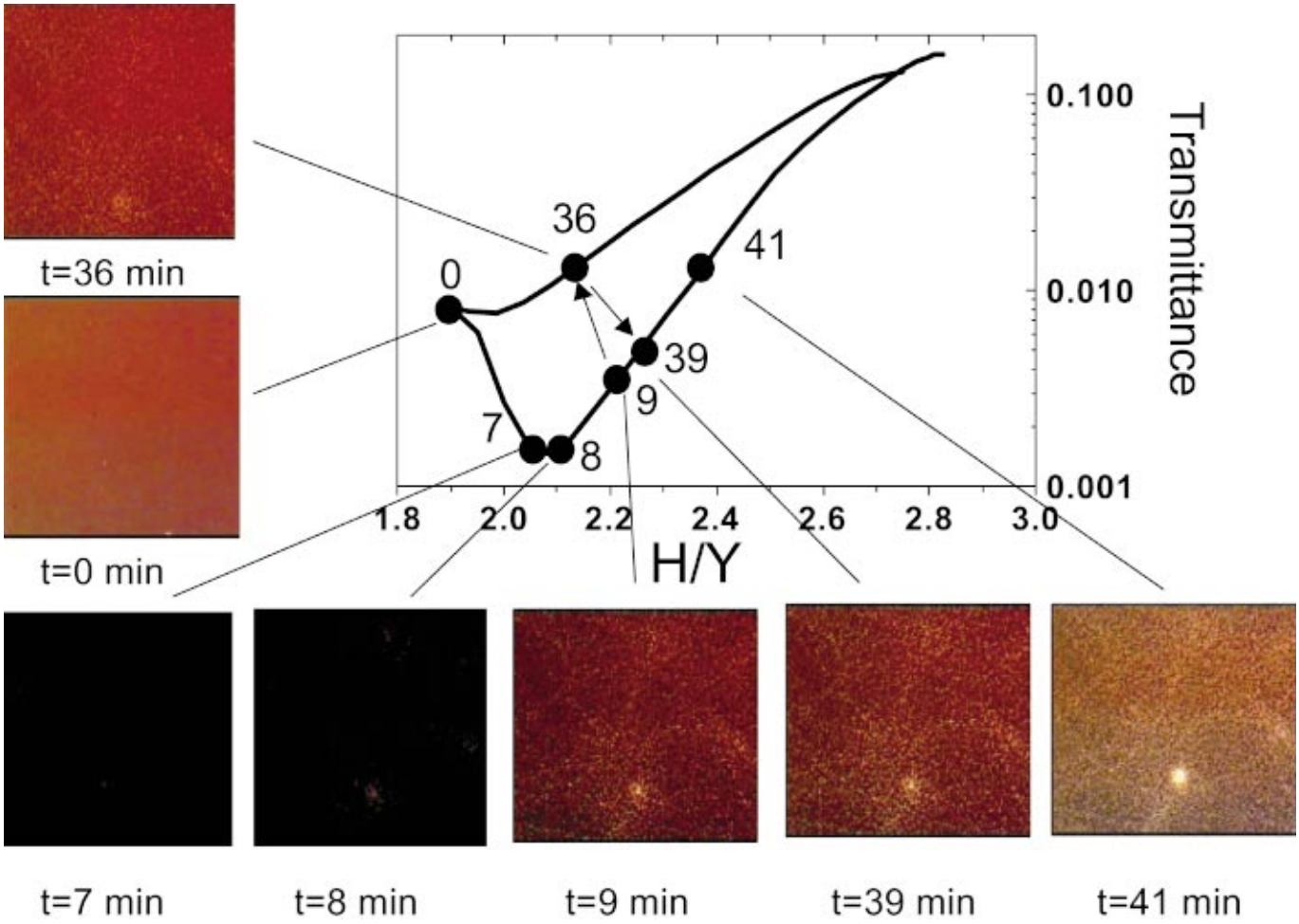

FIG. 6. (Color) Optical appearance in transmission of a 300 nm Y film capped with 10 nm Pd during a cycling sequence performed at a temperature of 70 °C and a hydrogen pressure of 50 mbar (loading). Each picture shows a $1.6\times1.2\,\mathrm{mm}^2$ area of the film. The initially homogeneously reddish film (at $t=0$) first becomes darker and at $t=8$ min a bright phase starts to nucleate at arbitrary places within the sample. This nucleation process continues as long as hydrogen is absorbed. After $t=9$ min the hydrogen gas is replaced by ambient air. Hydrogen desorps and the sample reaches a state on the upper leg of the hysteresis loop (compare also Fig. 1). At $t=36$ min the sample is again exposed to a hydrogen pressure of 50 mbar. Hydrogen is again absorbed and the sample reaches a state on the lower leg of the hysteresis loop. Note the different responses of the background and the bright spots.

affects first the β phase. The reddish transparent background gets darker before the nucleation of more domains of the transparent γ phase sets in. All images displayed in Fig. 6 are recorded under the same illumination conditions.

In a more quantitative way the process of loading, unloading and reloading can be followed by the individual brightness channels of the camera. For each recorded color (red, green, and blue) the brightness (photons per pixel) of an individual pixel is assigned to one of 256 brightness levels. Figure 7 displays the brightness histogram of the images in Fig. 6. At $t=0$ the distribution can be fitted with a single Gaussian function, centered around channel 46. With increasing time (i.e., hydrogen concentration) the darkening of the film results in a shift of the whole distribution function to lower channel numbers. At the same time the distribution sharpens and increases in intensity, leaving the area under the peak, thus the number of pixels constant. As soon as the first bright spots appear at $t=8$ min, the center of the distribution function stays at a constant value while a tail to higher channel numbers (higher brightness) develops. The curve can now be fitted with two Gaussian functions. One of them models the main peak, the second the tail.

Replacing the hydrogen atmosphere by ambient air at $t=9$ min causes hydrogen desorption and the main peak shifts back towards its initial value. Its area, i.e., the amount of pixels contributing to this peak does not change, as shown in Fig. 8. This corresponds nicely to the optical observation that during unloading the whole background gets brighter while the number of bright spots remains constant.

Reloading the film (at $t=36$ min) first reestablishes a dark background before more and more bright spots appear. Note that the brightness distribution of the bright spots is much wider than the width of the brightness distribution of the background. This has two reasons. First, the transmittance of the γ phase reacts very sensitive to the hydrogen concentration. As lateral diffusion is very slow, differences in hydrogen concentrations are not equilibrated rapidly, so that spatially separated domains may possess different hydrogen

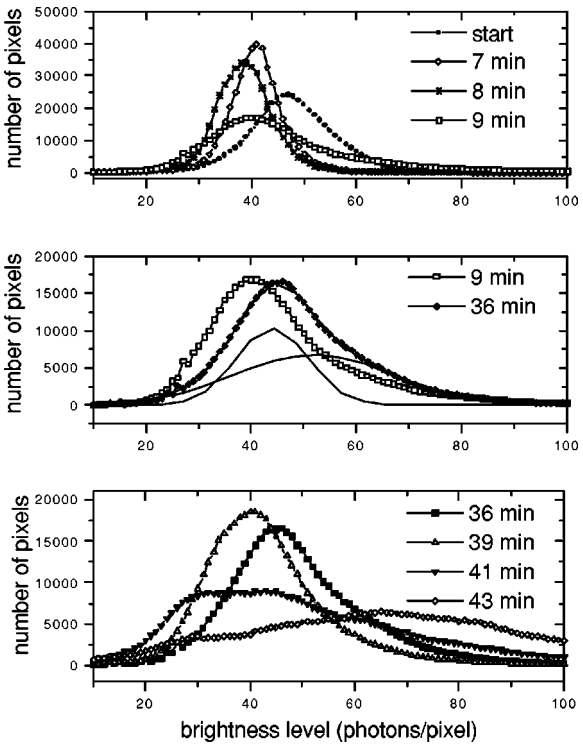

FIG. 7. Brightness distribution functions of the blue channel for the images displayed in Fig. 6. Top panel: hydrogen loading at 70 °C and a hydrogen pressure of 50 mbar from the initial state (start) to 9 min. Second panel: Unloading between $t=9$ min and $t=36$ min in ambient air at 70 °C. Bottom panel: Reloading in a hydrogen atmosphere of 50 mbar and at 70 °C between $t=36$ min and $t=43$ min. The channel number corresponds to the magnitude of the optical transmission, i.e., to the flux of photons per pixel.

concentrations. Second, the domain size is much smaller than the pixel size,[22] resulting in a quasicontinuous brightness distribution.

IV. DISCUSSION

The experimental results described above imply that upon hydrogen loading the sample remains in its cubic phase until

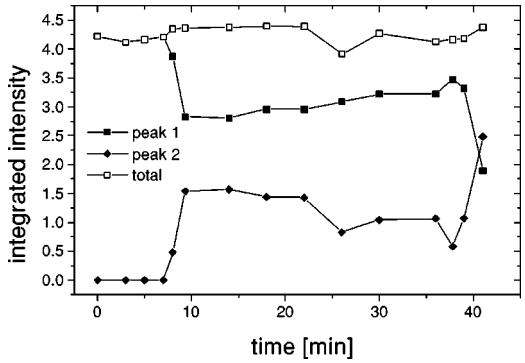

FIG. 8. The distribution functions in Fig. 7 can be fitted with two Gaussians, one representing the amount of the ''background'' phase in Fig. 6 (peak 1) and the other one representing the amount of the ''bright'' phase (peak 2). During unloading ($9\ \text{min} \leqslant t \leqslant 36\ \text{min}$) the ratio of the respective phases does not change.

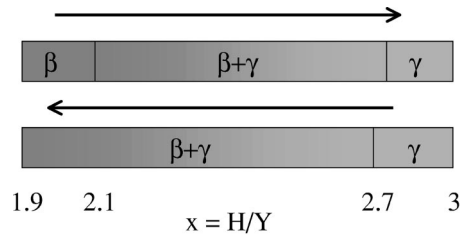

FIG. 9. Schematic phase diagram of polycrystalline thin YH_x films (typically 300 nm) at 70 °C during hydrogen loading (top) and unloading (bottom).

it reaches the phase boundary at $x=2.1$. For bulk YH_x the lattice parameter a of the cubic β-phase contracts with increasing x by[6]

$$\Delta a/a = -5\times10^{-5}\Delta x. \tag{1}$$

Assuming that Eq. (1) also holds for polycrystalline thin films, the observed contraction within the β phase corresponds to a concentration range of roughly $\Delta x=0.30\pm0.15$ within the cubic phase. The large error bar results from the polycrystalline nature of the sample and its small scattering volume. Nevertheless, this experiment proves the lattice contraction within the β phase and shows that the lattice parameter of the β phase (and thus of its hydrogen concentration) during phase coexistence depends on the history of the sample. The phase boundaries of the β phase can be deduced from electrochemical experiments in combination with the *in situ* measurements presented here. Identifying the minimum of the optical transmittance curve as the begin of the β-γ coexistence region, the upper solubility limit is at $x=2.1$, resulting in a β-phase concentration range of $\Delta x=0.2$. Below a hydrogen concentration of $x=2.1$ the sample is in one cubic crystal structure, and it appears optically homogeneous. In accordance with bulk data within this single phase the electrical resistivity and the optical transmittance vary with hydrogen concentration. As there are no spatial fluctuations in the optical images, it is reasonable to assume that the hydrogen concentration is homogeneous throughout the sample. At higher hydrogen concentrations the system enters the β-γ miscibility gap and the hexagonal γ phase nucleates at arbitrary places within the sample. It is difficult to conclude the exact hydrogen concentration within the γ-phase precipitates. While within the cubic β phase there is a clear relation between the hydrogen concentration and the lattice parameter, such a correlation is not found for the out-of-plane lattice parameter within the γ phase. Moreover, during hydrogen loading the solubility isotherm does not show a plateau which would clearly mark the miscibility gap. However, the electrical resistivity of 2 m Ω cm, measured at the moment where the system reaches structurally the pure γ phase corresponds to a hydrogen concentration of $x=2.7$. At the same value, the transmission-concentration hysteresis loop closes. Therefore, we conclude that $x=2.7$ is the low concentration limit for the hexagonal γ phase during loading.

During unloading the pressure composition isotherm reaches its plateau at $x=2.65$. Simultaneously the transmission-composition isotherm changes its slope. It is reasonable to assume that $x=2.65$ marks the low concentration limit of the γ phase during unloading. The resulting phase diagram at 70 °C is displayed in Fig. 9. The upper panel corresponds to hydrogen loading, the lower one to unloading.

At this point it is useful to compare our results with findings on epitaxial yttrium films. It has been demonstrated on epitaxial films that yttrium films undergo the β-γ structural transition domain-by-domain.[24,22] By means of *in situ* atomic force microscopy and optical microscopy the correlation between the expansion of a *c*-axis oriented domain (and thus its lattice parameter) and its optical transmittance could be demonstrated.[22] Concerning the morphology, the main differences between epitaxially grown films and *c*-axis textured polycrystalline films are the average domain size and in-plane orientation. In the case of epitaxial films micrometer sized domains are observed.[22] They are oriented along certain crystallographic axes of the substrate.[23,25] In *c*-axis textured polycrystalline films the domains are much smaller and randomly oriented. Individual domains could not be resolved optically in the present experiment. However, both kinds of films exhibit a similar hydrogen loading and unloading behavior. Optically and structurally the first occurrence of the γ phase is marked by the minimum of the averaged transmission. The hydrogen concentration at that specific point of the loading curve has been measured by electrochemical loading.[26] It is $x=2.1$, the bulk solubility limit of H in the β phase. Within the two-phase region the microscope image is no longer homogeneous. Large contrasts between highly transparent domains and a homogeneous background can be seen. Similar to structural domains observed by x-ray diffraction topography or the morphological domains detected by atomic force microscopy, the optical domains (''bright spots'') appear randomly on the sample, though there is a slight tendency for them to cluster.

The optical appearance as well as earlier results from AFM (Ref. 22) and x-ray diffraction topography[24] suggest a model in which columnar grains coexist next to each other, separated by grain boundaries. During hydrogenation the grain boundaries isolate the grains from each other. Each grain undergoes the phase transition individually.

The hysteresis in the transmission curves originates from the fact that during loading the γ phase coexists with the dark, high concentration β phase, while upon unloading the γ phase coexists with the low concentration fairly transparent β phase. Therefore, the structural transition plays a major role in the hysteretic behavior of thin yttrium-hydride films. Suppressing the structural transition by alloying lanthanum to the yttrium results in quenching of the hysteretic effects observed in pure yttrium films, as recently observed by van Gogh *et al.*[27]

This different behavior can be attributed to the different stress states during loading and unloading, as proposed by Dornheim *et al.*,[17] which lead to different solubility isotherms. Despite the fact that the unit cell volume of the hexagonal γ phase is about 10% larger than the unit cell volume of the cubic β phase, the in-plane lattice parameter of the γ phase is slightly smaller than the in-plane lattice parameter of the β phase. During loading the Y-Y distance within the basal plane first contracts from 3.684 to 3.666 Å before the system enters the miscibility gap,[6] thus reducing the compressive in-plane stress during phase coexistence. Additionally, the in-plane lattice parameter of the γ phase expands with increasing hydrogen pressure.[23] Therefore, in order to reduce the resulting mechanical stress, a high concentration γ phase is also favorable.

The smaller in-plane lattice constant of the γ phase during unloading refers to the lower hydrogen concentration of the γ phase during unloading. As the system also tries to avoid crossing the phase boundary, the γ phase unloads below its equilibrium value before the β phase nucleates. This lower concentration γ-phase contracts beyond its equilibrium value and is therefore under tensile stress. Precipitation of the expanded, low concentration β phase leads to compressive in-plane stress, stabilizing the low concentration γ phase.

Thus for both transitions, during loading and unloading, the occurring in-plane stresses can be used to explain the different hydrogen concentrations observed in the β phase, which lead to the hysteresis in pressure composition isotherms and electronic and optical properties.

V. CONCLUSIONS

Simultaneous measurements of optical transmittance, electrical resistivity and x-ray diffraction spectra confirm the presence of large hysteretic effects between the cubic β and the hexagonal γ phase in thin yttrium hydride films. Starting at a hydrogen concentration of $x=1.9$, the low concentration limit of the cubic β phase, the system retains its cubic symmetry up to a concentration of $x=2.1$. Further loading causes the system to cross the miscibility gap in which the cubic phase coexists with the hexagonal phase before hydrogen saturation is reached in the pure hexagonal phase. While the cubic phase stays at a concentration of $x=2.1$ in the coexistence region during loading it remains at a concentration of $x=1.9$ during unloading. The loading and unloading phase diagrams at 70 °C are shown in Fig. 9. The loading phase diagram is clearly different from that deduced by Kooij *et al.*[9] in a previous study of thin films. The hysteresis in optical transmission and in electrical resistivity is caused by the intrinsic concentration dependent properties of the cubic β phase. Our results can be interpreted on the basis of the bulk phase diagram by taking the different stress states during loading and unloading into account.

ACKNOWLEDGMENTS

We would like to thank A. Pundt, M. Dornheim, and B. Dam for fruitful discussions as well as N. J. Koeman for the careful preparation of the samples. This work was supported by the EU-TMR project ''Metal-hydride films with switchable physical properties,'' Project No. ERB FMRX-CT98-187, which we gratefully acknowledge.

[1] F. Klose, Ch. Rehm, D. Nagengast, H. Maletta, and A. Weidinger, Phys. Rev. Lett. **78**, 1150 (1997).
[2] B. Hjörvarsson, J. A. Dura, P. Isberg, T. Watanabe, T. J. Udovic, G. Andersson, and C. F. Majkrzak, Phys. Rev. Lett. **79**, 901 (1997).
[3] G. Song, A. Remhof, K. Theis-Bröhl, and H. Zabel, Phys. Rev. Lett. **79**, 5062 (1997).
[4] J. N. Huiberts, R. Griessen, J. H. Rector, R. J. Wijngaarden, J. P. Dekker, D. G. de Groot, and N. J. Koeman, Nature (London) **380**, 231 (1996).
[5] P. van der Sluis, M. Ouwerkerk, and P. A. Duine, Appl. Phys. Lett. **78**, 1315 (1997).
[6] P. Vadja, in *Handbook on the Physics and Chemistry of Rare Earth*, edited by K. A. Gschneidner and L. Eyring (Elsevier, Amsterdam, 1995), Vol. 20.
[7] M. Kremers, N. J. Koeman, R. Griessen, P. H. L. Notten, R. Tolboom, P. J. Kelly, and P. A. Duine, Phys. Rev. B **57**, 4943 (1998).
[8] R. W. G. Wyckoff, *Crystal Structures* (Interscience, New York, 1966), Vol. 1.
[9] E. S. Kooij, A. T. M. van Gogh, D. G. Nagengast, N. J. Koeman, and R. Griessen, Phys. Rev. B **62**, 10 088 (2000).
[10] J. H. Weaver, R. Rosei, and D. T. Peterson, Phys. Rev. B **19**, 4855 (1979); J. H. Weaver, D. T. Peterson, and R. L. Benbow, *ibid.* **20**, 5301 (1979).
[11] D. J. Peterman, B. N. Harmon, J. Marchiando, and J. H. Weaver, Phys. Rev. B **19**, 4867 (1979).
[12] T. J. Udovic, Q. Huang, and J. J. Rush, J. Phys. Chem. Solids **57**, 423 (1996); A. Remhof, G. Song, Ch. Sutter, A. Schreyer, R. Siebrecht, H. Zabel, F. Güthoff, and J. Windgasse, Phys. Rev. B **59**, 6689 (1999); T. J. Udovic, Q. Huang, R. W. Erwin, B. Hjörvarsson, and R. C. C. Ward, *ibid.* **61**, 12 701 (2000); P. van Gelderen, P. J. Kelly, and G. Brocks, *ibid.* **63**, 100301(R) (2001); H. Kierey, M. Rode, A. Jacob, A. Borgshulte, and J. Schönes, *ibid.* **63**, 134109 (2001).
[13] J. Shinar, B. Dehner, R. G. Barnes, and B. J. Beaudry, Phys. Rev. Lett. **64**, 563 (1990).
[14] A. F. Th. Hoekstra, A. S. Roy, T. F. Rosenbaum, R. Griessen, R. J. Wijngaarden, and N. J. Koeman, Phys. Rev. Lett. **86**, 5349 (2001).
[15] A. Remhof, G. Song, K. Theis-Bröhl, and H. Zabel, Phys. Rev. B **56**, R2897 (1997).
[16] J. Hayoz, S. Sarbach, T. Pillo, E. Boschung, D. Naumovic, P. Aebi, and L. Schlapbach, Phys. Rev. B **58**, R4270 (1998).
[17] M. Dornheim, A. Pundt, S. J. van der Molen, E. S. Kooij, J. W. J. Kerssemakers, H. Harms, U. Geyer, R. Griessen, and R. Kirchheim (unpublished).
[18] S. J. van der Molen, J. W. J. Kerssemakers, J. H. Rector, N. J. Koeman, B. Dam, and R. Griessen, J. Appl. Phys. **86**, 6107 (1999).
[19] L. J. van der Pauw, Philips Res. Rep. **13**, 1 (1958).
[20] S. Enache (private communication).
[21] M. Dornheim, A. Pundt, N. Jisrawi, E. S. Kooij, R. Griessen, and R. Kirchheim (unpublished).
[22] J. W. J. Kerssemakers, S. J. van der Molen, N. J. Koeman, R. Günter, and R. Griessen, Nature (London) **406**, 489 (2000).
[23] A. Remhof, G. Song, Ch. Sutter, A. Schreyer, R. Siebrecht, H. Zabel, F. Güthoff, and J. Windgasse, Phys. Rev. B **59**, 6689 (1999).
[24] A. Remhof, G. Song, C. Sutter, D. Labergerie, M. Hübener, H. Zabel, and J. Härtwig, Phys. Rev. B **62**, 2164 (2000).
[25] E. S. Kooij, J. H. Rector, D. Nagengast, J. W. J. Kerssemakers, B. Dam, R. Griessen, A. Remhof, and H. Zabel, Thin Solid Films **402**/1-2, 130 (2002).
[26] E. S. Kooij, A. T. M. van Gogh, and R. Griessen, J. Electrochem. Soc. **146**, 2990 (1999).
[27] A. T. M. van Gogh, D. G. Nagengast, E. S. Kooij, N. J. Koeman, and R. Griessen, Phys. Rev. Lett. **85**, 2156 (2000).